ATLAS NOTE

ATLAS-CONF-2012-012

March 5, 2012

Search for the Standard Model Higgs boson in the $H \to WW^{(*)} \to \ell\nu\ell\nu$ decay mode with 4.7 fb^{-1} of ATLAS data at $\sqrt{s} = 7$ TeV

The ATLAS Collaboration

Abstract

A Standard Model Higgs boson search in the $H \to WW^{(*)} \to \ell\nu\ell\nu$ ($\ell = e, \mu$) decay mode has been performed using proton-proton collision data corresponding to an integrated luminosity of 4.7 fb^{-1} at a centre-of-mass energy of 7 TeV collected during 2011 with the ATLAS detector at the Large Hadron Collider. No significant excess of observed events over the expected background is observed. An upper bound is placed on the Higgs boson production cross section as a function of its mass. A Standard Model Higgs boson with a mass in the range between 130 GeV and 260 GeV is excluded at a 95% confidence level, while the expected exclusion range is 127 GeV $\leq m_H \leq$ 234 GeV.

1 Introduction

The Higgs boson is the only particle in the Standard Model (SM) of particle physics that has not yet been observed. It is intimately related to the Higgs mechanism [1–3] which in the SM gives mass to all other massive elementary particles. The search for this particle is a centrepiece of the Large Hadron Collider (LHC) physics programme.

Indirect limits on the Higgs boson mass of $m_H < 185$ GeV at 95% confidence level (CL) have been set using global fits to electroweak precision results [4]. Direct searches at LEP and Tevatron have excluded at 95% CL a SM Higgs boson with a mass below 114.4 GeV [5] and in the region $156 < m_H < 177$ GeV [6], respectively.

The results of searches in various channels using data corresponding to an integrated luminosity of approximately 5 fb^{-1} of data have recently been reported by both the ATLAS and CMS collaborations [7, 8], excluding the mass range between 112.9 and 115.5 GeV and the region between 127 GeV and 600 GeV.

In the $H \to WW^{(*)} \to \ell\nu\ell\nu$ channel, ATLAS reported the results of a search using 2.05 fb^{-1} of data, which excluded a SM Higgs boson in the mass ranges between 145 GeV $< m_H <$ 206 GeV at 95% CL [9]. This note extends the analysis of Ref. [9] using data corresponding to an integrated luminosity of 4.7 fb^{-1} of pp collisions at $\sqrt{s} = 7$ TeV recorded in 2011, with modified selections to gain sensitivity at low m_H and to cope with increased instantaneous luminosities. The sensitivity is further enhanced by expanding the selection to include events with two jets, and by considering the kinematic distributions of the events satisfying the selection criteria.

The data and simulated samples are briefly summarised in Section 2. Section 3 describes the event selections for the different jet multiplicity analyses. Sources of systematic uncertainty are discussed in Section 4. Section 5 details the use of data control samples to estimate the dominant backgrounds. Finally, Section 6 presents the results of this analysis.

2 Data and Simulated Samples

The data used for this analysis were collected in 2011 using the ATLAS detector, a multipurpose particle physics experiment with a forward-backward symmetric cylindrical geometry and near 4π coverage in solid angle [10]. It consists of an inner tracking detector surrounded by a thin superconducting solenoid, electromagnetic and hadronic calorimeters, and an external muon spectrometer incorporating three large superconducting air-core toroid magnets. In particular, it allows charged particle, electron, muon, and jet reconstruction and identification up to pseudorapidities[1] $|\eta| = 2.5$, 2.5, 2.7, and 4.9, respectively. An accurate reconstruction of missing transverse momentum, $E_{\mathrm{T}}^{\mathrm{miss}}$, is made possible by the good hermeticity of the detector.

The data were collected using inclusive single-muon and single-electron triggers. The single muon trigger required the transverse momentum of the muon with respect to the beam line, p_{T}, to exceed 18 GeV; for the single-electron trigger, the threshold varied from 20 to 22 GeV. The trigger object quality requirements were tightened throughout the data taking period to cope with the increasing instantaneous luminosity.

In this analysis, the signal contributions that are considered include the dominant gluon fusion

[1] ATLAS uses a right-handed coordinate system with its origin at the nominal interaction point (IP) in the centre of the detector and the z-axis along the beam pipe. The x-axis points from the IP to the centre of the LHC ring, and the y axis points upwards. Cylindrical coordinates (r, ϕ) are used in the transverse plane, ϕ being the azimuthal angle around the beam pipe. The pseudorapidity is defined in terms of the polar angle θ as $\eta = -\ln\tan(\theta/2)$.

production process ($gg \rightarrow H$, denoted as ggF) and the vector boson fusion production process ($qq' \rightarrow qq'H$, denoted as VBF). For the decay of the Higgs boson, only the $H \rightarrow WW^{(*)} \rightarrow \ell\nu\ell\nu$ mode is considered. The branching fraction for this decay is taken from the HDECAY [11] program.

The signal cross sections are computed up to next-to-next-to-leading order (NNLO) [12–17] in QCD for the ggF process. Next-to-leading order (NLO) electroweak (EW) corrections are also applied [18, 19] as well as QCD soft-gluon resummations up to next-to-next-to-leading log (NNLL). These results improve the NNLO calculation [20] and are detailed in Refs. [21–23], assuming factorisation between QCD and EW corrections. Full NLO QCD and EW corrections [24–26] and approximate NNLO QCD corrections [27] are used to calculate the cross sections for VBF signal production.

The ggF and VBF processes are modelled using the POWHEG [28, 29] Monte Carlo (MC) generator, interfaced to PYTHIA [30] for showering and hadronisation; the ggF Higgs boson p_{T} spectrum is reweighted to agree with the prediction from HqT [31].

ALPGEN [32], interfaced to HERWIG [33] with the MLM matching scheme [34] is used to model the production of W and Z/γ^* bosons decaying to charged leptons in association with jets. MC@NLO [35] is used to model $t\bar{t}$ and WW production, using HERWIG for the parton hadronisation; an additional contribution to the continuum WW background from gluon-initiated diagrams is modelled using gg2WW [36] interfaced with HERWIG. Wherever parton showering is performed by HERWIG, JIMMY [37] is used for the simulation of the underlying event. SHERPA [38] is used for the generation ZZ final states while MC@NLO is chosen for WZ production. $W\gamma$ production is modelled with ALPGEN while MADGRAPH [39] is employed for $W\gamma^*$ [40]. AcerMC [41] is used for the generation of single top events in all three production channels (s-channel, t-channel, and Wt).

The CT10 PDF set [42] is used for the MC@NLO samples, CTEQ6L1 [43] for the ALPGEN, SHERPA, and MADGRAPH samples, and MRSTMCal [44] for the PYTHIA samples. Acceptances and efficiencies are based on a full simulation of the ATLAS detector using GEANT4 [45, 46]. This includes a realistic treatment of the event pile-up conditions present in the 2011 data; from the first 2.1 fb^{-1} to the last 2.6 fb^{-1} of data taken, the average number of interactions per bunch crossing increased from 5.7 to 10.8. The data are affected by the detector response to multiple proton-proton interactions occurring in the same or in different bunch crossings.

3 Event Selection

Events are required to have a primary vertex that is consistent with the beam spot position, with at least three associated tracks with $p_{\mathrm{T}} > 400$ MeV. Overall quality criteria are applied in order to suppress non-collision backgrounds such as cosmic-ray muons, beam-related backgrounds, or noise in the calorimeters.

$H \rightarrow WW^{(*)} \rightarrow \ell\nu\ell\nu$ candidates are pre-selected by requiring exactly two oppositely charged leptons with p_{T} thresholds of 25 GeV and 15 GeV for the leading and sub-leading lepton, respectively. For muons, the full acceptance is used; for electrons, the region $1.37 < |\eta| < 1.52$ is excluded. The selected electron candidates are reconstructed using a combination of tracking and calorimetric information [47], while the muon candidates are identified by matching tracks reconstructed in the inner detector and in the muon spectrometer. At least one of the selected leptons is required to match a triggering object. Leptons from heavy-flavour decays and jets satisfying the lepton identification criteria are suppressed by requiring the leptons to be isolated: the scalar sum of the p_{T} of charged particles and of the calorimeter energy deposits within $\Delta R = \sqrt{\Delta\phi^2 + \Delta\eta^2} = 0.3$ of the lepton direction is required to be less than approximately 0.15 times the lepton p_{T}.

The Drell-Yan production of Z/γ^* or Υ resonances leads to two same-flavour, opposite-sign high-p_{T} leptons. In the ee and $\mu\mu$ channels (the channels are indicated by the lepton flavours), this background is suppressed by requiring the dilepton invariant mass to be greater than 12 GeV, and to differ from the Z-boson mass m_Z by at least 15 GeV. For the $e\mu$ channel, the dilepton invariant mass is required to be greater than 10 GeV.

The remaining QCD multijet and Drell-Yan events are suppressed by requiring large $E_{\mathrm{T}}^{\mathrm{miss}}$. The $E_{\mathrm{T}}^{\mathrm{miss}}$ is the magnitude of $\boldsymbol{p}_{\mathrm{T}}^{\mathrm{miss}}$, the opposite of the vector sum of the reconstructed objects' transverse momenta, including muons, electrons, photons, jets, and calorimeter clusters not associated with these objects. The quantity $E_{\mathrm{T,rel}}^{\mathrm{miss}}$ used in this analysis is defined as: $E_{\mathrm{T,rel}}^{\mathrm{miss}} = E_{\mathrm{T}}^{\mathrm{miss}} \sin\Delta\phi_{\mathrm{min}}$, with $\Delta\phi_{\mathrm{min}} \equiv \min(\Delta\phi, \frac{\pi}{2})$. Here, $\Delta\phi$ is the absolute azimuthal angular difference between the $E_{\mathrm{T}}^{\mathrm{miss}}$ vector and the nearest candidate lepton or jet with $p_{\mathrm{T}} > 25$ GeV. For the ee and $\mu\mu$ channels, multijet production via QCD processes, in the following referred to as QCD background, and Drell-Yan events are suppressed by requiring $E_{\mathrm{T,rel}}^{\mathrm{miss}} > 45$ GeV. For the $e\mu$ channel, where Drell-Yan background originates predominantly from the $\tau\tau$ production channel, this cut is lowered to $E_{\mathrm{T,rel}}^{\mathrm{miss}} > 25$ GeV. After the $E_{\mathrm{T,rel}}^{\mathrm{miss}}$ cut, the QCD background is found to be negligible. As can be observed in Fig. 1, the $E_{\mathrm{T,rel}}^{\mathrm{miss}}$ variable is described well by the predicted backgrounds. For this Figure, all the backgrounds are estimated using the MC simulation except the W+jets background which is estimated using a data-driven approach.

Figure 2 shows the multiplicity distribution of jets reconstructed using the anti-k_t algorithm [48] with distance parameter $R = 0.4$, for all events satisfying the pre-selection criteria described above. The backgrounds are estimated with the MC simulation except for W+jets which is estimated using a data-driven approach, and the WW, top, and Drell Yan backgrounds which are normalized to data in control regions. Only jets with $p_{\mathrm{T}} > 25$ GeV and $|\eta| < 4.5$ are counted. This threshold is increased to 30 GeV in the region $2.75 < |\eta| < 3.25$, which corresponds to a boundary between two calorimeter systems and is more sensitive to reconstruction issues arising from pile-up. The background rate and composition depend significantly on jet multiplicity, as does the signal topology: without accompanying jets the signal is dominated by the ggF process, while in the presence of two or more jets the signal receives a large contribution from the VBF process. To maximise the sensitivity, further selection criteria that depend on the jet multiplicity are applied to the sample defined by the pre-selection criteria described previously. In detail, the data are subdivided into $H+0$, $H+1$, and $H+2$-jet channels according to the jet counting defined above, with the $H+2$-jet channel also including higher jet multiplicities. The different selections for these channels are described in more detail below.

Due to spin correlations in the $WW^{(*)}$ system arising from the spin-0 nature of the Higgs boson, the charged leptons tend to emerge from the interaction point in the same direction. This kinematic feature is exploited in all jet multiplicities by requiring that the azimuthal angular difference between the leptons, $\Delta\phi_{\ell\ell}$, be less than 1.8 radians, and that the dilepton invariant mass, $m_{\ell\ell}$, be less than 50 GeV for the $H+0$-jet and $H+1$-jet channels. For the $H+2$-jet channel, the $m_{\ell\ell}$ upper bound is increased to 80 GeV for the $e\mu$ channel and $m_Z - 15$ GeV for the same-flavour channels. For $m_H \geq 200$ GeV, the leptons tend to have higher p_{T} and larger angular separation. Therefore, the $\Delta\phi_{\ell\ell}$ cut is omitted and only a $m_{\ell\ell} < 150$ GeV criterion is retained, with the exclusion of the mass region $|m_{\ell\ell} - m_Z| < 15$ GeV in the ee and $\mu\mu$ final states. For $m_H > 300$ GeV, the $m_{\ell\ell} < 150$ GeV criterion is also omitted. In the following, the selections for $m_H < 200$ GeV, 200 GeV $\leq m_H \leq 300$ GeV, and $m_H > 300$ GeV are referred to as low m_H, intermediate m_H, and high m_H selections, respectively.

In the $H+0$-jet channel, the transverse momentum of the dilepton system, $p_{\mathrm{T}}^{\ell\ell}$, is required to be greater than 30 GeV for the $e\mu$ channel and greater than 45 GeV for the ee and $\mu\mu$ channels. This improves the rejection of Drell-Yan background.

In the $H+1$-jet channel, backgrounds from top quark decays are suppressed by rejecting any

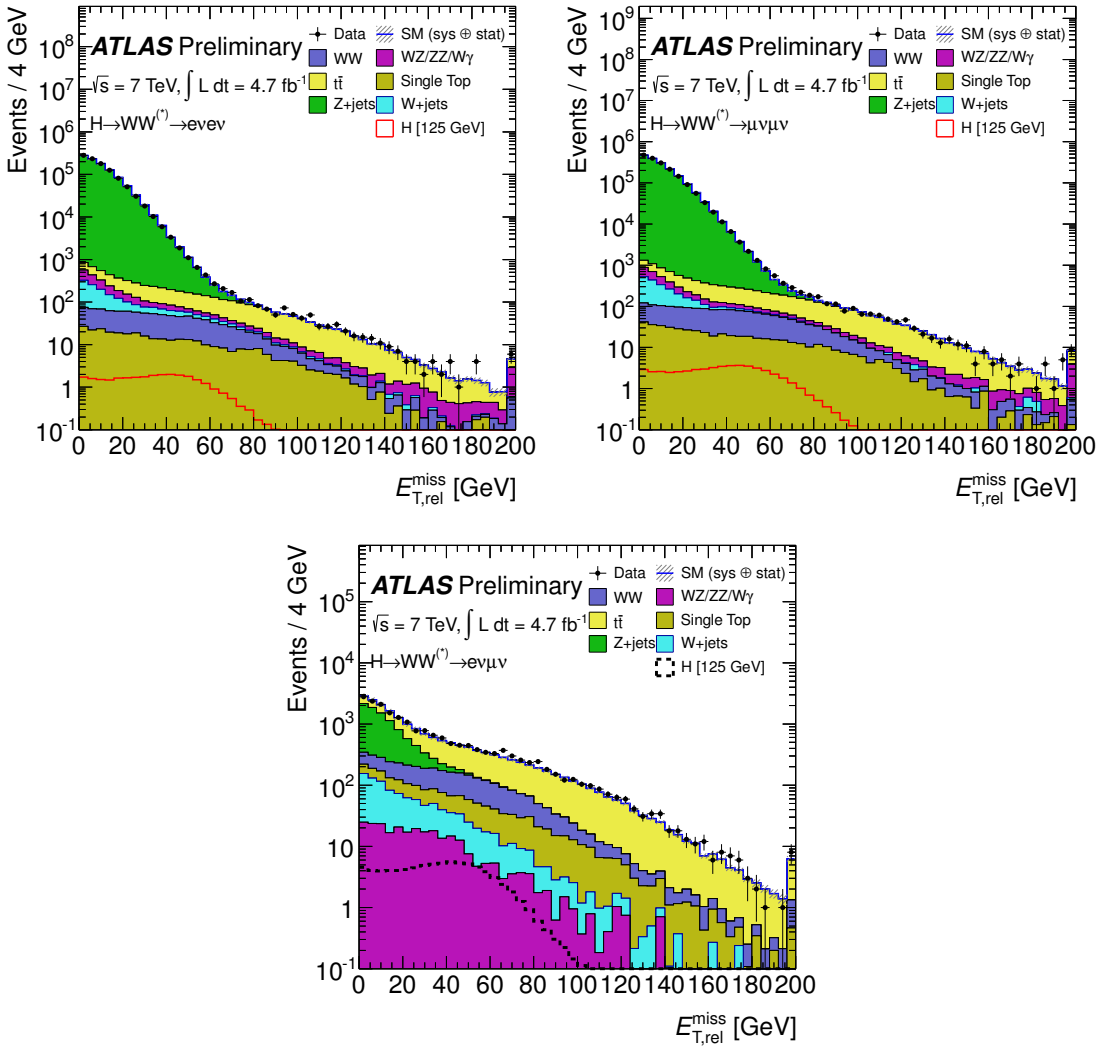

Figure 1: The $E_{\mathrm{T,rel}}^{\mathrm{miss}}$ distributions for the ee (top left), $\mu\mu$ (top right), and $e\mu$ (bottom) channels with the minimum lepton p_{T} and $m_{\ell\ell}$ requirements applied. The expected signal for a SM Higgs boson is shown for $m_H = 125$ GeV. The final bin includes the overflow.

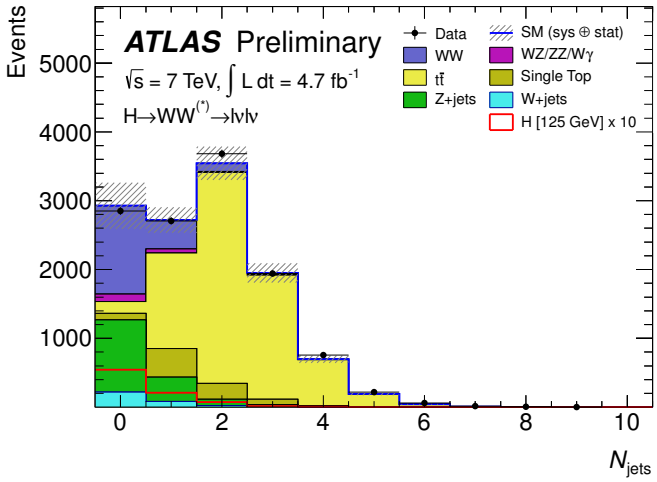

Figure 2: Multiplicity of jets within the acceptance described in the text, after the cut on $E_{\mathrm{T,rel}}^{\mathrm{miss}}$. The shaded region indicates the total uncertainty on the background prediction. The expected signal for a SM Higgs boson with $m_H = 125$ GeV is superimposed, multiplied by a factor of 10 for better readability.

event containing a b-tagged jet, as determined using a b-tagging algorithm which uses a combination of impact parameter significance and secondary vertexing information and exploits the topology of weak b- and c-hadron decays [49]. The algorithm is tuned to achieve an 80% b-jet identification efficiency while yielding a light-jet tagging rate of approximately 6% [50]. The total momentum, $p_{\mathrm{T}}^{\mathrm{tot}}$, defined as the magnitude of the vector sum $\mathbf{p}_{\mathrm{T}}^{\mathrm{tot}} = \mathbf{p}_{\mathrm{T}}^{\ell 1} + \mathbf{p}_{\mathrm{T}}^{\ell 2} + \mathbf{p}_{\mathrm{T}}^{\mathrm{j}} + \mathbf{p}_{\mathrm{T}}^{\mathrm{miss}}$, is required to be smaller than 30 GeV to suppress background events with jets with p_T below threshold. The $\tau\tau$ invariant mass, $m_{\tau\tau}$, is computed under the assumption that the reconstructed leptons are τ lepton decay products, that the neutrinos produced in the τ decays are collinear with the leptons [51], and that they are the only source of $E_{\mathrm{T}}^{\mathrm{miss}}$. Events with $|m_{\tau\tau} - m_Z| < 25$ GeV are rejected if the energy fractions carried by the putative visible decay products are positive[2].

The $H+$ 2-jet selection follows the $H+$ 1-jet selection described above (with the $p_{\mathrm{T}}^{\mathrm{tot}}$ definition modified to include the second jet). In addition, the following jet-related cuts are applied: the two highest-p_{T} jets in the event, the "tag" jets, are required to lie in opposite rapidity hemispheres ($\eta_{\mathrm{j1}} \times \eta_{\mathrm{j2}} < 0$); the two jets must be separated in pseudorapidity by a distance $|\Delta\eta_{\mathrm{jj}}|$ of at least 3.8 units; the invariant mass of the two tag jets, m_{jj}, must be at least 500 GeV; finally, there must be no additional jets within $|\eta| < 3.2$.

A transverse mass variable, m_{T} [52], is used in this analysis to test for the presence of a signal. This variable is defined as:

$$m_{\mathrm{T}} = \sqrt{(E_{\mathrm{T}}^{\ell\ell} + E_{\mathrm{T}}^{\mathrm{miss}})^2 - |\mathbf{p}_{\mathrm{T}}^{\ell\ell} + \mathbf{p}_{\mathrm{T}}^{\mathrm{miss}}|^2},$$

where $E_{\mathrm{T}}^{\ell\ell} = \sqrt{|\mathbf{p}_{\mathrm{T}}^{\ell\ell}|^2 + m_{\ell\ell}^2}$, $|\mathbf{p}_{\mathrm{T}}^{\mathrm{miss}}| = E_{\mathrm{T}}^{\mathrm{miss}}$, and $|\mathbf{p}_{\mathrm{T}}^{\ell\ell}| = p_{\mathrm{T}}^{\ell\ell}$. The predicted number of events from background sources at each stage of the selection procedure outlined above is presented in Table 1. Figure 3 shows the distributions of the transverse mass after all selection criteria in the $H+$ 0-jet and

[2]The collinear approximation does not always yield good solutions.

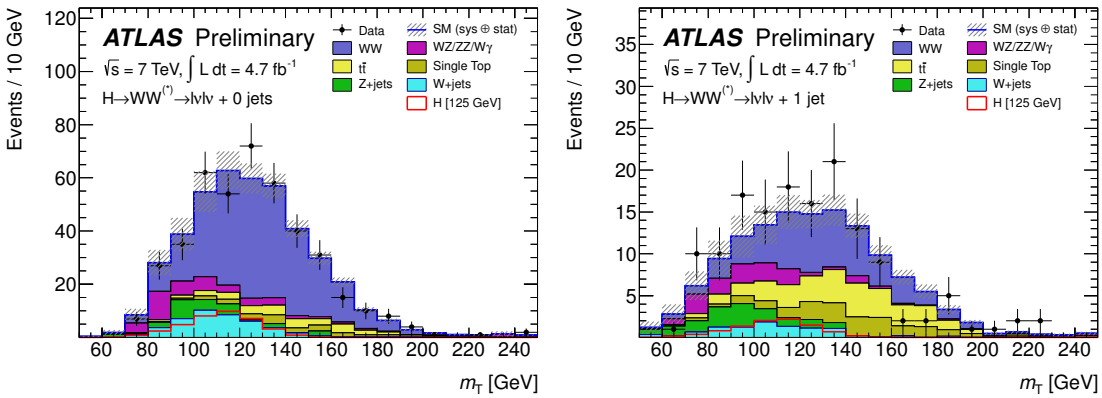

Figure 3: Transverse mass, m_{T}, distribution in the $H+$ 0-jet (left) and $H+$ 1-jet (right) channels, for events satisfying all criteria for the low m_H selection. The lepton flavours are combined. The expected signal for a SM Higgs boson with $m_H = 125$ GeV is superimposed. The hashed area indicates the total uncertainty on the background prediction.

$H+$ 1-jet analyses, for all lepton flavours combined. No distribution is shown for the $H+$ 2-jet channel as only a single event is selected in the data. The backgrounds are estimated with the MC simulation except for W+jets which is estimated using a data-driven approach, and the WW, top, and Drell-Yan backgrounds which are normalised to data in control regions.

4 Systematic Uncertainties

Theoretical uncertainties on the signal production cross sections are determined following Refs. [53, 54]. QCD renormalisation and factorisation scales are varied up and down independently by a factor of two. Independent uncertainties on ggF signal production are assumed for the inclusive cross section and the cross section for production with at least one or two jets. The resulting relative uncertainties on the exclusive ggF signal cross sections depend on m_H, rising from ±25% (±37%) at 125 GeV and 240 GeV to ±47% (±43%) at 600 GeV for $H+$ 0-jet ($H+$ 1-jet) analyses [54–56]. The uncertainty on the VBF signal cross section and on the acceptance associated with the jet veto requirement, to which the $H+$ 2-jet analysis is mainly sensitive, varies from ±5% at 125 GeV to ±6 % at 600 GeV. In the $H+$ 2-jet channel, around 25% of the signal events are produced via ggF, where the uncertainty on the ggF signal cross section in the $H+$ 2-jet analysis is around 25%. An additional uncertainty due to the Higgs line shape description in the POWHEG Monte Carlo is added in quadrature for both the ggF and the VBF channel and amounts to $150\% \times (m_H/1\ \mathrm{TeV})^3$ [54, 57–59]. PDF uncertainties are estimated, following Refs. [42, 60–62], by considering their respective error sets applied separately to quark-quark, quark-gluon, and gluon-gluon initiated processes. The relative PDF uncertainty on the dominant ggF signal process is about 8% while the associated VBF uncertainty is included in the values reported above. Uncertainties on the modelling of processes are estimated by using alternative generators, such as ALPGEN for WW production, POWHEG for the $t\bar{t}$ process, and MC@NLO for the ggF process. The uncertainties associated with the underlying event and parton showering are taken into account in the acceptance error, although they are negligible with respect to the scale uncertainties on the jet binning.

The main experimental uncertainties are related to the jet energy scale. It is determined from

a combination of test beam, simulation, and *in situ* measurements, and is below 14% for jets with $p_{\mathrm{T}} > 25$ GeV and $|\eta| < 4.5$ [63]. An additional contribution from pile-up is estimated to be below 5% for jets with $p_{\mathrm{T}} > 25$ GeV. The uncertainty on the jet energy resolution is estimated from *in situ* measurements. Electron and muon (reconstruction, identification and trigger) efficiencies and their momentum scale and resolution are estimated using $Z \to \ell\ell$, $J/\psi \to \ell\ell$, and $W \to \ell\nu$ decays ($\ell = e, \mu$). With the exception of the uncertainty on the electron efficiency, which varies between 5% and 2% as a function of p_{T} and η, the resulting uncertainties are all smaller than 1% and are negligible. Jet energy scale and lepton momentum scale uncertainties are propagated to the $E_{\mathrm{T}}^{\mathrm{miss}}$ computation. Additional uncertainties arise from jets with $p_{\mathrm{T}} < 20$ GeV as well as from soft calorimeter energy deposits not associated with reconstructed physics objects [64]. Finally, $E_{\mathrm{T}}^{\mathrm{miss}}$ uncertainties arising from pile-up contributions are estimated by varying the modelling of pile-up interactions. The efficiency of the b-tagging criterion is calibrated using samples featuring muons produced in the vicinity of jets [50]. The resulting uncertainty on the b-jet tagging efficiency varies between 5% and 14%, as a function of jet p_{T}. The uncertainty on the integrated luminosity estimate is 3.9% [65, 66].

In this analysis, a fit to the m_{T} distribution is performed in order to obtain the signal yield for each mass hypothesis. None of the theoretical and experimental uncertainties on individual backgrounds or on the signal exhibits a m_{T} dependence with any appreciable effect on the results. Hence, the shape variation of the total background is dominated by the normalisation variation of the individual backgrounds.

Note that the uncertainties listed above do not account for the use of control regions in data, as described below.

5 Background Normalisation and Control Samples

The dominant backgrounds are normalised using control samples obtained from the data with similar selections as those used in the signal region but with some criteria reversed or modified to create signal-depleted, background-enriched regions. In the following, such control samples are defined for the WW, Z/γ^*+jets, top, and W+jets backgrounds.

5.1 WW control sample

The WW background MC prediction is normalised using a control region defined with the same selection as for the signal region except that the $\Delta\phi_{\ell\ell}$ requirement is removed. In addition, the upper selection on $m_{\ell\ell}$ is replaced with a lower bound $m_{\ell\ell} > 80$ GeV ($m_{\ell\ell} > m_Z + 15$ GeV) for the $e\mu$ (ee and $\mu\mu$) final states. Figure 4 shows the m_{T} distributions in this control region in the $H+$ 0-jet and $H+$ 1-jet analyses. The number of events in the WW control region in data agrees well with the MC predictions, as can be seen in Table 1. The total uncertainty on the predicted WW background in the signal region is 10% and 24% for the 0 and 1-jet selections, respectively.

This control region is used only for the low m_H selection in the $H+$ 0-jet and $H+$ 1-jet analyses. In the intermediate ($200 < m_H < 300$) and high ($m_H > 300$) m_H selections, or in the $H+$ 2-jet analysis, a high-statistics signal-depleted region cannot be isolated in this fashion; in these cases, the MC prediction is used.

5.2 Z/γ^*+jets control sample

In the ee and $\mu\mu$ final states and separately in the $H+$ 0-jet and $H+$ 1-jet analyses, a Z/γ^*+jets control region is constructed, after application of all selection criteria except that on $\Delta\phi_{\ell\ell}$, by considering a

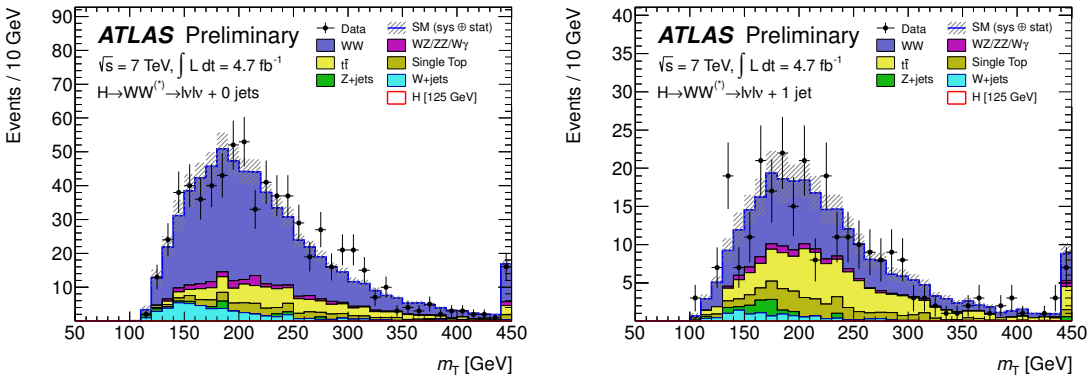

Figure 4: Distributions of the m_{T} variable in the WW control regions in the $H+$ 0-jet (left) and $H+$ 1-jet (right) analyses. The lepton flavours are combined. The signal shown is for $m_H = 125$ GeV. The hashed area indicates the total uncertainty on the background prediction. The final bin includes the overflow.

region with a modified criterion, 20 GeV $< E_{\mathrm{T,rel}}^{\mathrm{miss}} <$ 45 GeV. The number of events in this region, with non-Z/γ^*+jets contributions subtracted using MC, is scaled by the ratio of event counts in the $E_{\mathrm{T,rel}}^{\mathrm{miss}} >$ 45 GeV and 20 GeV $< E_{\mathrm{T,rel}}^{\mathrm{miss}} <$ 45 GeV regions for $|m_{\ell\ell} - m_Z| <$ 15 GeV. Simulated events have been used to validate the assumption that the scale factor is independent of $m_{\ell\ell}$. The acceptance of the $\Delta\phi_{\ell\ell}$ selection criterion is taken from simulation.

In the $e\mu$ channel of the $H+$ 0-jet analysis, the background is estimated using the MC simulation and cross-checked with data using a control region dominated by $Z \to \tau\tau$ decays, which is constructed by requiring 10 GeV $< m_{\ell\ell} <$ 80 GeV, $\Delta\phi_{\ell\ell} > 2.5$, and $p_{\mathrm{T}}^{\ell\ell} <$ 30 GeV. A $E_{\mathrm{T,rel}}^{\mathrm{miss}}$ threshold of 25 GeV is used to calculate the scale factor, matching the cut applied to this channel in the nominal cutflow. The resulting scale factor is consistent with unity within uncertainties. Owing to the difficulty of constructing a control region for higher jet multiplicities, a similar cross-check cannot be performed for the $H+$ 1-jet and $H+$ 2-jet analyses.

The uncertainty on this background amounts to 56% and 25% in events with no jets and one jet, respectively.

5.3 Top control sample

In the $H+$ 0-jet signal region, the estimated number of top background events is extrapolated from the number of events satisfying the pre-selection criteria. This sample is dominated by top backgrounds, as shown in Fig. 2. Corrections for non-top sources are applied; the double-jet veto probability obtained from simulation is corrected with the squared ratio of single jet veto probabilities in data and simulation, as determined in an another control sample selected by requiring at least one b-jet in addition to the pre-selection criteria [67]. The overall efficiency for the requirements on $p_{\mathrm{T}}^{\ell\ell}$, $m_{\ell\ell}$, and $\Delta\phi_{\ell\ell}$ is taken from simulation. The total uncertainty on the top background estimate in events with no jets is 23%.

In the $H+$ 1-jet and $H+$ 2-jet analyses, the top background MC prediction is normalised to the data using a control sample defined by reversing the b-jet veto and removing the requirements on $\Delta\phi_{\ell\ell}$ and $m_{\ell\ell}$. The resulting samples are dominated by top backgrounds (both $t\bar{t}$ and single-top production), with little contribution from other sources. The number of events in the 1-jet control region is given in Table 1. The total uncertainty on the estimated top background in the $H+$ 1-jet and $H+$ 2-jet analyses

amounts to approximately 30%.

Figure 5 shows the corresponding m_{T} distribution for the H+1-jet analysis. In the H+2-jet analysis a different control region is defined by requiring a b-tagged jet after the central jet veto selection; this control region is selected in order to increase the sample size used to make comparisons between the MC prediction and the data.

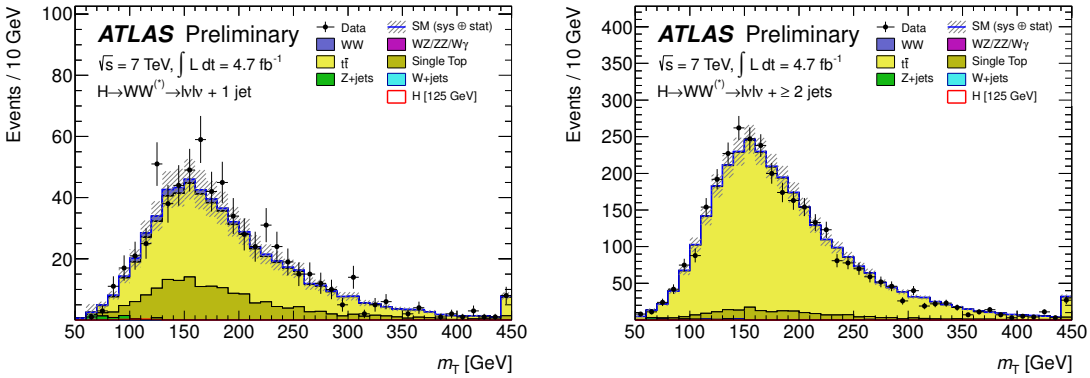

Figure 5: Distributions of the m_{T} variable in a top control region defined by requiring a b-tagged jet after the central jet veto selection, in the $H+$ 1-jet (left) and $H+$ 2-jet (right) analyses. The lepton flavours are combined. The signal shown is for $m_H = 125$ GeV. The hashed area indicates the total uncertainty on the background prediction. The final bin includes the overflow.

5.4 W+jets control sample

The W+jets background contribution is estimated using a data control sample of events where one of the two leptons satisfies the identification and isolation criteria described in Section 3, and the other lepton (denoted "anti-identified") fails these criteria while satisfying a loosened selection. The W+jets contamination in the signal region is then obtained by scaling the number of events in the data control sample by a normalisation "fake factor". The fake factor is estimated as a function of anti-identified lepton p_{T} using an inclusive dijet data sample, with residual contributions from real leptons arising from leptonic W and Z decays removed. The W candidates are identified by requiring the transverse mass $m_{\mathrm{T}}^{W} = \sqrt{2p_{\mathrm{T}}^{\ell}p_{\mathrm{T}}^{\mathrm{miss}} \cdot (1 - \cos\Delta\phi)}$ to satisfy $m_{\mathrm{T}}^{W} > 30$ GeV. In this expression, p_{T}^{ℓ} is the lepton transverse momentum and $\Delta\phi$ is the difference in azimuth between the lepton and the missing transverse momentum direction. The Z candidates are identified requiring two opposite-sign leptons of the same flavour and $|m_{\ell\ell} - m_Z| < 15$ GeV. The small remaining lepton contamination is subtracted using MC simulation. The dominant contribution to this background comes from fake electrons. The fake factor uncertainty is the main uncertainty on the W+jets background contribution. The components of this uncertainty include: trigger bias, data sample dependence, and the subtraction of the contribution from real leptons from leptonic W and Z decays. The total uncertainty on the fake factor is estimated to be 30–50% for lepton $p_{\mathrm{T}} < 30$ GeV and of the order of 100% for $p_{\mathrm{T}} > 30$ GeV. The background predicted for this process in the $H+$ 2-jet channels is negligible.

6 Results

The expected numbers of signal ($m_H = 125$ GeV) and background events at several stages of the selection are presented in Table 1. The rightmost column shows the observed numbers of events in the data. The uncertainties reflect only the limited statistics of the MC samples and of the control samples used to normalise the dominant backgrounds. After all selection criteria, the dominant background in the $H+$ 0-jet channel comes from continuum WW production, with smaller contributions from top ($t\bar{t}$ and single top) and W+jets events. In the $H+$ 1-jet and $H+$ 2-jet channels, the WW and top backgrounds are comparable.

Table 1: The expected numbers of signal and background events after the requirements for the low m_H selection listed in the first column, as well as the observed numbers of events in data. The signal is for $m_H = 125$ GeV. The W+jets background is entirely determined from data, whereas for the other processes the expectations are based on simulation, with WW, Z/γ^*+jets, $t\bar{t}$, and $tW/tb/tqb$ normalised using the data control regions as described in the text. Only statistical uncertainties associated with the number of events in the MC samples and the data control regions are shown. The same numbers are shown also in the control regions; here, with the exception of W+jets, no normalisation scale factors are applied to the expected numbers. The bottom part of the table lists the number of expected and observed events for each lepton channel after the $\Delta\phi_{\ell\ell}$ cut.

H + 0-jet	Signal	WW	$WZ/ZZ/W\gamma$	$t\bar{t}$	$tW/tb/tqb$	Z/γ^* + jets	W + jets	Total Bkg.	Obs.
Jet Veto	54.5 ± 0.2	1285 ± 79	106 ± 6	175 ± 12	95 ± 7	1038 ± 28	217 ± 4	2916 ± 115	2851
$m_{\ell\ell} < 50$ GeV	43.8 ± 0.2	316 ± 20	48 ± 5	30 ± 2	19 ± 2	157 ± 13	69 ± 2	640 ± 34	644
$p_{\mathrm{T}}^{\ell\ell}$ cut	38.8 ± 0.2	285 ± 18	41 ± 4	28 ± 2	18 ± 2	24 ± 7	49 ± 2	444 ± 27	441
$\Delta\phi_{\ell\ell} < 1.8$	37.7 ± 0.2	279 ± 17	39 ± 4	27 ± 2	18 ± 2	23 ± 7	44 ± 1	429 ± 27	427
H + 1-jet	Signal	WW	$WZ/ZZ/W\gamma$	$t\bar{t}$	$tW/tb/tqb$	Z/γ^* + jets	W + jets	Total Bkg.	Obs.
1 jet	21.1 ± 0.1	390 ± 55	59 ± 4	1433 ± 80	430 ± 25	357 ± 17	82 ± 3	2752 ± 170	2707
b-jet veto	19.5 ± 0.1	360 ± 51	55 ± 4	401 ± 23	134 ± 8	333 ± 16	73 ± 3	1356 ± 92	1371
$\lvert\mathbf{p}_{\mathrm{T}}^{\mathrm{tot}}\rvert < 30$ GeV	13.0 ± 0.1	252 ± 35	33 ± 3	171 ± 10	78 ± 5	105 ± 8	35 ± 2	674 ± 55	685
$Z \to \tau\tau$ veto	13.0 ± 0.1	246 ± 34	32 ± 3	165 ± 10	75 ± 5	85 ± 7	35 ± 2	638 ± 53	645
$m_{\ell\ell} < 50$ GeV	10.2 ± 0.1	54 ± 7	14 ± 2	32 ± 2	18 ± 2	26 ± 4	12 ± 1	156 ± 14	171
$\Delta\phi_{\ell\ell} < 1.8$	9.4 ± 0.1	49 ± 7	14 ± 2	30 ± 2	17 ± 2	13 ± 3	10 ± 1	134 ± 13	145
H + 2-jet	Signal	WW	$WZ/ZZ/W\gamma$	$t\bar{t}$	$tW/tb/tqb$	Z/γ^* + jets	W + jets	Total Bkg.	Obs.
opp. hemispheres	3.8 ± 0.1	46 ± 1	6 ± 1	138 ± 3	21 ± 1	34 ± 4	8 ± 1	253 ± 5	269
$\lvert\Delta\eta_{\mathrm{jj}}\rvert > 3.8$	1.8 ± 0.1	8.3 ± 0.4	0.9 ± 0.2	19.2 ± 0.9	2.2 ± 0.4	8.0 ± 2.0	1.5 ± 0.4	40.2 ± 2.3	40
$m_{\mathrm{jj}} > 500$ GeV	1.3 ± 0.1	3.9 ± 0.3	0.4 ± 0.1	6.9 ± 0.4	0.7 ± 0.2	0.9 ± 0.4	0.7 ± 0.3	13.6 ± 0.8	13
$m_{\ell\ell} < 80$ GeV	0.9 ± 0.1	1.1 ± 0.2	0.1 ± 0.1	1.1 ± 0.2	0.2 ± 0.1	0.3 ± 0.3	0.2 ± 0.2	2.9 ± 0.5	2
$\Delta\phi_{\ell\ell} < 1.8$	0.8 ± 0.1	0.7 ± 0.1	0.1 ± 0.1	0.7 ± 0.2	negl.	0.3 ± 0.3	negl.	1.8 ± 0.4	1
Control Regions	Signal	WW	$WZ/ZZ/W\gamma$	$t\bar{t}$	$tW/tb/tqb$	Z/γ^* + jets	W + jets	Total Bkg.	Obs.
WW 0-jet	0.1 ± 0.1	465 ± 3	25 ± 2	85 ± 2	41 ± 2	9 ± 2	48 ± 2	673 ± 5	698
WW 1-jet	0.1 ± 0.1	126 ± 2	10 ± 1	83 ± 2	33 ± 2	9 ± 2	11 ± 1	272 ± 4	269
Top 1-jet	1.1 ± 0.1	21 ± 1	1.5 ± 0.2	422 ± 4	165 ± 3	6 ± 2	negl.	615 ± 6	675

Lepton Channels	0-jet ee	0-jet $\mu\mu$	0-jet $e\mu$	1-jet ee	1-jet $\mu\mu$	1-jet $e\mu$
Total bkg.	58 ± 5	114 ± 10	257 ± 13	21 ± 3	37 ± 5	76 ± 6
Signal	3.8 ± 0.1	9.0 ± 0.1	25 ± 0.2	1.1 ± 0.1	2.3 ± 0.1	6.0 ± 0.1
Observed	52	138	237	19	36	90

Table 2 shows the numbers of events expected from signal and background and observed in data, after application of all selection criteria. To reflect better the sensitivity of the analysis, an additional

mass-dependent cut on m_{T} is applied. The results are shown for all lepton flavours combined. The uncertainties shown in this table include those of Table 1 as well as the systematic uncertainties discussed in Section 4, but are constrained by the use of the control regions discussed in Section 5. The uncertainties are those that enter into the fitting procedure described below.

Table 2: The expected numbers of signal (m_H = 125 GeV and 240 GeV) and background events after the full low m_H and intermediate m_H selections, including a cut on the transverse mass of $0.75\,m_H < m_{\mathrm{T}} < m_H$ for m_H = 125 GeV and $0.6\,m_H < m_{\mathrm{T}} < m_H$ for m_H = 240 GeV. The observed numbers of events in data are also displayed. The uncertainties shown are the combination of the statistical and all systematic uncertainties, taking into account the constraints from control samples. Note that these results and uncertainties differ from those discussed earlier also due the application of the additional m_{T} criterion. All numbers are summed over lepton flavours.

		Signal	WW	$WZ/ZZ/W\gamma$	$t\bar{t}$	$tW/tb/tqb$	Z/γ^* + jets	W + jets	Total Bkg.	Obs.
0-jet	m_H = 125 GeV	25 ± 7	110 ± 12	12 ± 3	7 ± 2	5 ± 2	13 ± 8	27 ± 16	173 ± 22	174
	m_H = 240 GeV	60 ± 17	432 ± 49	24 ± 3	68 ± 15	39 ± 9	8 ± 2	36 ± 24	607 ± 63	629
1-jet	m_H = 125 GeV	6 ± 2	18 ± 3	6 ± 3	7 ± 2	4 ± 2	6 ± 1	5 ± 3	45 ± 7	56
	m_H = 240 GeV	23 ± 9	99 ± 22	8 ± 1	73 ± 27	35 ± 19	6 ± 2	7 ± 7	229 ± 55	232
2-jet	m_H = 125 GeV	0.4 ± 0.2	0.3 ± 0.2	negl.	0.2 ± 0.1	negl.	0.0 ± 0.1	negl.	0.5 ± 0.2	0
	m_H = 240 GeV	2.5 ± 0.6	1.1 ± 0.7	0.1 ± 0.1	2.6 ± 1.3	0.3 ± 0.3	negl.	0.1 ± 0.1	4.2 ± 1.7	2

The statistical analysis of the data employs a binned likelihood function $\mathcal{L}(\mu, \boldsymbol{\theta})$ constructed as the product of Poisson probability terms in each lepton flavour channel. The H+ 0-jet (H+ 1-jet) signal regions are further subdivided into five (three) m_{T} bins. For the H+ 2-jet signal region, and the WW and top control regions, only the results integrated over m_{T} are used; no shape information is used due to the small number of events remaining after selections. Because of event pile-up conditions changing throughout data taking and leading to a progressively worsening $E_{\mathrm{T}}^{\mathrm{miss}}$ resolution, separate likelihood terms are constructed for the first 2.1 fb^{-1} used already in Ref. [9], and the remaining 2.6 fb^{-1} dataset. A "signal strength" parameter, μ, multiplies the expected signal from the Standard Model in each bin. Signal and background predictions depend on systematic uncertainties that are parametrised by nuisance parameters $\boldsymbol{\theta}$, which in turn are constrained using Gaussian functions. The expected signal and background event counts in each bin are functions of $\boldsymbol{\theta}$. The parametrisation is chosen such that the rates in each channel are log-normally distributed for a normally distributed θ. The test statistic q_μ is then constructed using the profile likelihood: $q_\mu = -2\ln\Big(\mathcal{L}(\mu, \hat{\hat{\boldsymbol{\theta}}}_\mu)/\mathcal{L}(\hat{\mu}, \hat{\boldsymbol{\theta}})\Big)$, where $\hat{\mu}$ and $\hat{\boldsymbol{\theta}}$ are the parameters that maximise the likelihood (with the constraint $0 \leq \hat{\mu} \leq \mu$), and $\hat{\hat{\boldsymbol{\theta}}}_\mu$ corresponds to the conditional maximum likelihood of $\boldsymbol{\theta}$ for a given μ. This test statistic is used to compute exclusion limits following the modified frequentist method known as CL$_s$ [68, 69].

Figure 6 shows, as a function of m_H, the observed and expected cross section upper limits at 95% CL, for the combined H+ 0-jet, H+ 1-jet and H+ 2-jet analyses. No significant excess of events over the expected background is observed over the entire mass range. A Standard Model Higgs boson with a mass in the range from 130 GeV to 260 GeV is excluded at 95% CL while the expected exclusion range is 127 GeV $\leq m_H \leq$ 234 GeV.

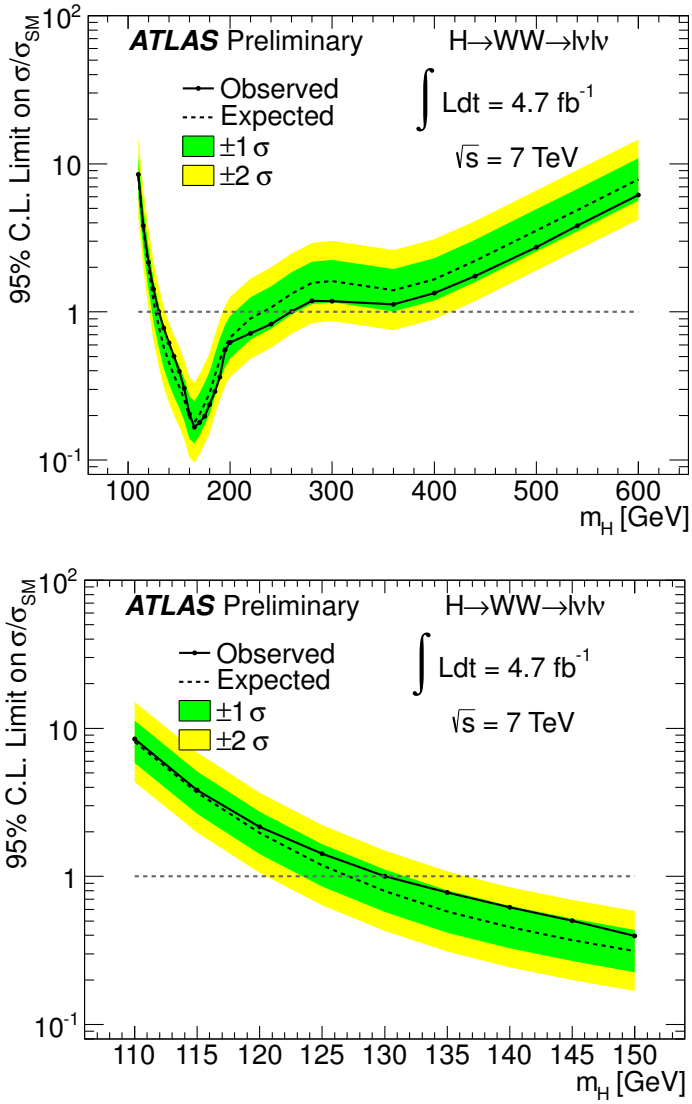

Figure 6: Expected (dashed) and observed (solid) 95% CL upper limits on the cross section, normalised to the SM cross section, as a function of m_H, over the full mass range considered in this analysis (top) and restricted to the range $m_H < 150$ GeV (bottom). The green and yellow regions indicate the $\pm 1\sigma$ and $\pm 2\sigma$ uncertainty bands on the expected limit, respectively. The results at neighbouring mass points are highly correlated due to the limited mass resolution in this final state.

7 Conclusion

A search for the SM Higgs boson has been performed in the $H \to WW^{(*)} \to \ell\nu\ell\nu$ channel using 4.7 fb^{-1} of pp collision data at $\sqrt{s}$ = 7 TeV recorded with the ATLAS detector. No significant excess of events over the expected background has been observed. A Standard Model Higgs boson with a mass in the range from 130 GeV to 260 GeV is excluded at 95% CL, while the expected exclusion range is 127 GeV $\leq m_H \leq$ 234 GeV.

References

[1] F. Englert and R. Brout, *Broken symmetry and the mass of gauge vector mesons*, Phys. Rev. Lett. **13** (1964) 321.

[2] P. W. Higgs, *Broken symmetries and the masses of gauge bosons*, Phys. Rev. Lett. **13** (1964) 508.

[3] G. S. Guralnik, C. R. Hagen, and T. W. B. Kibble, *Global conservation laws and massless particles*, Phys. Rev. Lett. **13** (1964) 585.

[4] The ALEPH, DELPHI, L3, OPAL, SLD, CDF, and DØ Collaborations, and the LEP Tevatron SLD Electroweak Working Group. CERN-PH-EP-2010-095, 2010. arXiv:1012.2367 [hep-ex].

[5] LEP Working Group for Higgs boson searches, *Search for the Standard Model Higgs boson at LEP*, Phys. Lett. **B565** (2003) 61, arXiv:hep-ex/0306033.

[6] The CDF and DØ Collaborations, and the Tevatron New Phenomena and Higgs Working Group, *Combined CDF and D0 upper limits on Standard Model Higgs boson production with up to 8.6 fb^{-1} of data*, arXiv:1107.5518 (2011) .

[7] ATLAS Collaboration, *Combined search for the Standard Model Higgs boson using up to 4.9 fb^{-1} of pp collision data at $\sqrt{s} = 7$ TeV with the ATLAS detector at the LHC*, arXiv:1202.1408 [hep-ex].

[8] CMS Collaboration, *Combined results of searches for the Standard Model Higgs boson in pp collisions at $\sqrt{s} = 7$ TeV*, arXiv:1202.1488 [hep-ex].

[9] ATLAS Collaboration, *Search for the Higgs boson in the $H \to WW^{(*)} \to \ell\nu\ell\nu$ decay channel in pp collisions at $\sqrt{s} = 7$ TeV with the ATLAS detector*, arXiv:1112.2577 [hep-ex].

[10] ATLAS Collaboration, *The ATLAS experiment at the CERN Large Hadron Collider*, JINST **3** (2008) S08003.

[11] A. Djouadi, J. Kalinowski, and M. Spira, *HDECAY: A program for Higgs boson decays in the Standard Model and its supersymmetric extension*, Comput. Phys. Commun. **108** (1998) 56, arXiv:hep-ph/9704448.

[12] A. Djouadi, M. Spira, and P. M. Zerwas, *Production of Higgs bosons in proton colliders: QCD corrections*, Phys. Lett. **B264** (1991) 440.

[13] S. Dawson, *Radiative corrections to Higgs boson production*, Nucl. Phys. **B359** (1991) 283.

[14] M. Spira, A. Djouadi, D. Graudenz, and P. M. Zerwas, *Higgs boson production at the LHC*, Nucl. Phys. **B453** (1995) 17, hep-ph/9504378.

[15] R. Harlander and W. B. Kilgore, *Next-to-next-to-leading order Higgs production at hadron colliders*, Phys. Rev. Lett. **88** (2002) 201801, arXiv:hep-ph/0201206 [hep-ph].

[16] C. Anastasiou and K. Melnikov, *Higgs boson production at hadron colliders in NNLO QCD*, Nucl. Phys. **B646** (2002) 220, arXiv:hep-ph/0207004 [hep-ph].

[17] V. Ravindran, J. Smith, W. L. van Neerven, *NNLO corrections to the total cross section for Higgs boson production in hadron hadron collisions*, Nucl. Phys. **B665** (2003) 325, arXiv:hep-ph/0302135 [hep-ph].

[18] U. Aglietti, R. Bonciani, G. Degrassi, and A. Vicini, *Two loop light fermion contribution to Higgs production and decays*, Phys. Lett. **B595** (2004) 432, arXiv:hep-ph/0404071 [hep-ph].

[19] S. Actis, G. Passarino, C. Sturm, and S. Uccirati, *NLO electroweak corrections to Higgs boson production at hadron colliders*, Phys. Lett. **B670** (2008) 12, arXiv:0809.1301 [hep-ph].

[20] S. Catani, D. de Florian, M. Grazzini, and P. Nason, *Soft-gluon re-summation for Higgs boson production at hadron colliders*, JHEP **0307** (2003) 028, arXiv:hep-ph/0306211.

[21] C. Anastasiou, R. Boughezal, and F. Petriello, *Mixed QCD-electroweak corrections to Higgs boson production in gluon fusion*, JHEP **0904** (2009) 003, arXiv:0811.3458 [hep-ph].

[22] D. de Florian and M. Grazzini, *Higgs production through gluon fusion: Updated cross sections at the Tevatron and the LHC*, Phys. Lett. **B674** (2009) 291, arXiv:0901.2427 [hep-ph].

[23] J. Baglio and A. Djouadi, *Higgs production at the LHC*, JHEP **1103** (2011) 055, arXiv:1012.0530 [hep-ph].

[24] M. Ciccolini, A. Denner, and S. Dittmaier, *Strong and electroweak corrections to the production of Higgs+2jets via weak interactions at the LHC*, Phys. Rev. Lett. **99** (2007) 161803, arXiv:0707.0381 [hep-ph].

[25] M. Ciccolini, A. Denner, and S. Dittmaier, *Electroweak and QCD corrections to Higgs production via vector-boson fusion at the LHC*, Phys. Rev. **D77** (2008) 013002, arXiv:0710.4749 [hep-ph].

[26] K. Arnold, M. Bahr, G. Bozzi, F. Campanario, C. Englert, et al., *VBFNLO: A parton level Monte Carlo for processes with electroweak bosons*, Comput.Phys.Commun. **180** (2009) 1661, arXiv:0811.4559 [hep-ph].

[27] P. Bolzoni, F. Maltoni, S.-O. Moch, and M. Zaro, *Higgs production via vector-boson fusion at NNLO in QCD*, Phys. Rev. Lett. **105** (2010) 011801, arXiv:arXiv:1003.4451 [hep-ph].

[28] S. Alioli, P. Nason, and C. Oleari, and E. Re, *NLO Higgs boson production via gluon fusion matched with shower in POWHEG*, JHEP **0904** (2009) 002, arXiv:0812.0578 [hep-ph].

[29] P. Nason and C. Oleari, *NLO Higgs boson production via vector-boson fusion matched with shower in POWHEG*, JHEP **1002** (2010) 037, arXiv:0911.5299 [hep-ph].

[30] T. Sjostrand, S. Mrenna, and P. Z. Skands, *PYTHIA 6.4 physics and manual*, JHEP **0605** (2006) 026.

[31] D. de Florian et al., *Transverse-momentum resummation: Higgs boson production at the Tevatron and the LHC*, JHEP **11** (2011) 064, arXiv:1109.2109 [hep-ph]. For Higgs boson $p_{\mathrm{T}} > m_H$, the calculation is switched from NLO+NLL to NLO.

[32] M. L. Mangano et al., *ALPGEN, a generator for hard multi-parton processes in hadronic collisions*, JHEP **0307** (2003) 001.

[33] G. Corcella et al., *HERWIG 6: An event generator for hadron emission reactions with interfering gluons (including super-symmetric processes)* , JHEP **0101** (2001) 010.

[34] J. Alwall et al., *Comparative study of various algorithms for the merging of parton showers and matrix elements in hadronic collisions*, Eur. Phys. J. **C53** (2008) 473.

[35] S. Frixione and B. R. Webber, *Matching NLO QCD computations and parton shower simulations*, JHEP **06** (2002) 029, arXiv:hep-ph/0204244.

[36] N. K. T. Binoth, M. Ciccolini and M. Kramer, *Gluon-induced W-boson pair production at the LHC*, JHEP **0612** (2006) 046, hep-ph/0611170v1.

[37] J. M. Butterworth, J. R. Forshaw, and M. H. Seymour, *Multiparton interactions in photoproduction at HERA*, Z. Phys. **C72** (1996) 637–646, arXiv:hep-ph/9601371.

[38] T. Gleisberg et al., *Event generation with SHERPA 1.1*, JHEP **0902** (2009) 007, arXiv:0811.4622 [hep-ph].

[39] J. Alwall et al., *MadGraph/MadEvent v4: The new web generation*, JHEP **0709** (2007) 028, arXiv:0706.2334 [hep-ph].

[40] R. C. Gray, C. Kilic, M. Park, S. Somalwar, and S. Thomas, *Backgrounds To Higgs boson searches from $W\gamma^* \to lvl(l)$ asymmetric internal conversion*, arXiv:1110.1368 [hep-ph].

[41] B. P. Kersevan and E. Richter-Was, *The Monte Carlo event generator AcerMC version 2.0 with interfaces to PYTHIA 6.2 and HERWIG 6.5*, arXiv:hep-ph/0405247 (2004) .

[42] H.-L. Lai et al., *New parton distributions for collider physics*, Phys. Rev. **D82** (2010) 074024, arXiv:1007.2241 [hep-ph].

[43] P. M. Nadolsky et al., *Implications of CTEQ global analysis for collider observables*, Phys. Rev. **D78** (2008) 013004.

[44] A. Sherstnev and R. S. Thorne, *Parton distributions for the LHC*, Eur. Phys. J **C55** (2009) 553.

[45] S. Agostinelli et al., *GEANT 4, a simulation toolkit*, Nucl. Instrum. Meth. **A506** (2003) 250.

[46] ATLAS Collaboration, *The ATLAS simulation infrastructure*, Eur. Phys. J. **C70** (2010) 823, arXiv:1005.4568 [physics.ins-det].

[47] ATLAS Collaboration, *Electron performance measurements with the ATLAS detector using the 2010 LHC proton-proton collision data*, arXiv:1110.3174 [hep-ex]. subm. to Eur. Phys. J. C.

[48] M. Cacciari, G. P. Salam, and G. Soyez, *Anti-k_t jet clustering algorithm*, JHEP **0804** (2008) 063, arXiv:0802.1189.

[49] ATLAS Collaboration, *Commissioning of the ATLAS high-performance b-tagging algorithms in the 7 TeV collision data*, ATLAS-CONF-2011-102 (2011) .

[50] ATLAS Collaboration, *Calibrating the b-tag efficiency and mistag rate in 35 pb^{-1} of data with the ATLAS detector*, ATLAS-CONF-2011-089 (2011) .

[51] R.K. Ellis et al., *Higgs decay to $\tau^+\tau^-$: A possible signature of intermediate mass Higgs bosons at the SSC*, Nucl. Phys. B **297** (1988) 221.

[52] A. J. Barr, B. Gripaios, and C. G. Lester, *Measuring the Higgs boson mass in dileptonic W-boson decays at hadron colliders*, JHEP **0907** (2009) 072, arXiv:0902.4864 [hep-ph].

[53] LHC Higgs Cross Section Working Group, S. Dittmaier, C. Mariotti, G. Passarino, and R. T. (Eds.), *Handbook of LHC Higgs cross sections: 1. Inclusive observables*, arXiv:1101.0593 (2011) .

[54] LHC Higgs Cross Section Working Group, S. Dittmaier, C. Mariotti, G. Passarino, and R. Tanaka (Eds.), *Handbook of LHC Higgs cross sections: 2. Differential distributions*, arXiv:1201.3084 (2012) .

[55] I. Stewart and F. Tackmann, *Theory uncertainties for Higgs mass and other searches using jet bins*, Phys. Rev. **D85** (2012) 034011, arXiv:1107.2117 [hep-ph].

[56] ATLAS and CMS Collaboration, *Procedure for the LHC Higgs boson search combination in summer 2011*, ATL-PHYS-PUB-2011-011, CMS-NOTE-2011-005 (2011) .

[57] M. H. Seymour, *The Higgs boson line shape and perturbative unitarity*, Phys.Lett. **B354** (1995) 409–414, arXiv:hep-ph/9505211 [hep-ph].

[58] G. Passarino, C. Sturm, and S. Uccirati, *Higgs Pseudo-Observables, Second Riemann Sheet and All That*, Nucl.Phys. **B834** (2010) 77–115, arXiv:1001.3360 [hep-ph].

[59] C. Anastasiou, S. Buehler, F. Herzog, and A. Lazopoulos, *Total cross-section for Higgs boson hadroproduction with anomalous Standard Model interactions*, JHEP **1112** (2011) 058, arXiv:1107.0683 [hep-ph].

[60] M. Botje et al., *The PDF4LHC working group interim recommendations*, arXiv:1101.0538 (2011) .

[61] A. D. Martin, W. J. Stirling, R. S. Thorne, and G. Watt, *Parton distributions for the LHC*, Eur. Phys. J. **C63** (2009) 189, arXiv:0901.0002 [hep-ph].

[62] R. D. Ball, V. Bertone, F. Cerutti, L. D. Debbio, S. Forte, et al., *Impact of heavy quark masses on parton distributions and LHC phenomenology*, Nucl. Phys. **B849** (2011) 296, hep-ph/11011300.

[63] ATLAS Collaboration, *Jet energy measurement with the ATLAS detector in proton-proton collisions at $\sqrt{s} = 7$ TeV*, arXiv:1112.6426 [hep-ex].

[64] ATLAS Collaboration, *Performance of missing transverse momentum reconstruction in proton-proton collisions at 7 TeV with ATLAS*, Eur. Phys. J. **C72** (2012) 1844, arXiv:1108.5602 [hep-ex].

[65] ATLAS Collaboration, *Luminosity Determination in pp Collisions at $\sqrt{s} = 7$ TeV Using the ATLAS Detector at the LHC*, Eur.Phys.J. **C71** (2011) 1630, arXiv:1101.2185 [hep-ex].

[66] ATLAS Collaboration, *Luminosity determination in pp collisions at $\sqrt{s} = 7$ TeV using the ATLAS detector in 2011*, ATLAS-CONF-2011-116 (2011) .

[67] B. Mellado, X. Ruan, and Z. Zhang, *Extraction of top backgrounds in the Higgs boson search with the $H \to WW^\star \to \ell\ell + E_{\mathrm{T}}^{\mathrm{miss}}$ decay with a full-jet veto at the LHC*, Phys.Rev. **D84** (2011) 096005, arXiv:1101.1383 [hep-ph].

[68] A.L. Read, *Presentation of search results: the CL_s technique*, J. Phys. G **28** (2002) 2693.

[69] G. Cowan, K. Cranmer, E. Gross, and O. Vitells, *Asymptotic formulae for likelihood-based tests of new physics*, Eur. Phys. J. **C71** (2011) 1554.

A Additional Figures

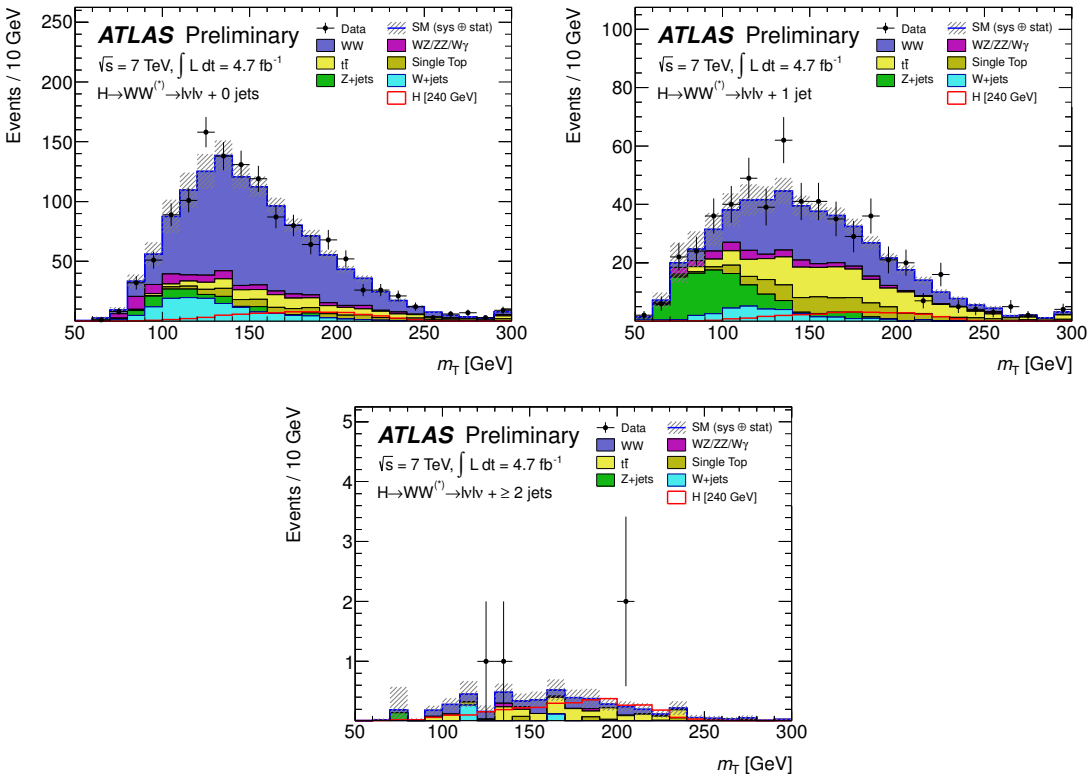

Figure 7: Transverse mass, m_{T}, distribution in the H+0-jet (top left), H+1-jet (top right) and H+2-jet (bottom) channels, for events satisfying all intermediate m_H selection criteria. The lepton flavours are combined. The hashed area indicates the total uncertainty on the background prediction. The signal shown is for $m_H = 240$ GeV. The final bin includes the overflow.

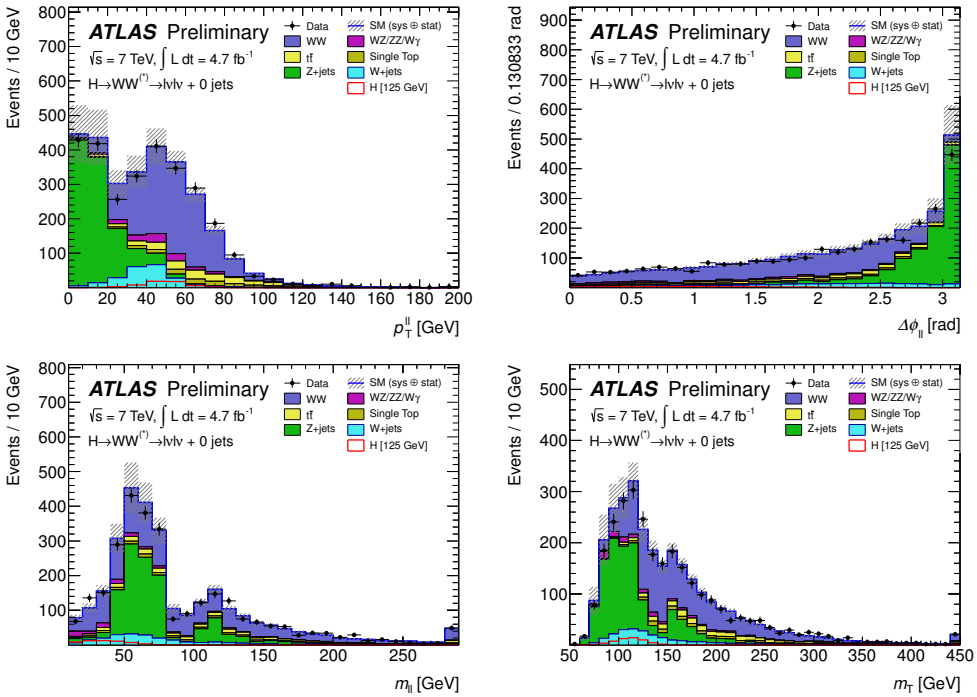

Figure 8: Kinematic distributions in the $H+0$-jet channel, before the application of the $m_{\ell\ell}$ cut: $p_{\mathrm{T}}^{\ell\ell}$ (top left), $\Delta\phi_{\ell\ell}$ (top right), $m_{\ell\ell}$ (bottom left), m_{T} (bottom right). The lepton flavours are combined. The signal shown is for $m_H = 125$ GeV. The hashed area indicates the total uncertainty on the background prediction. The final bin includes the overflow.

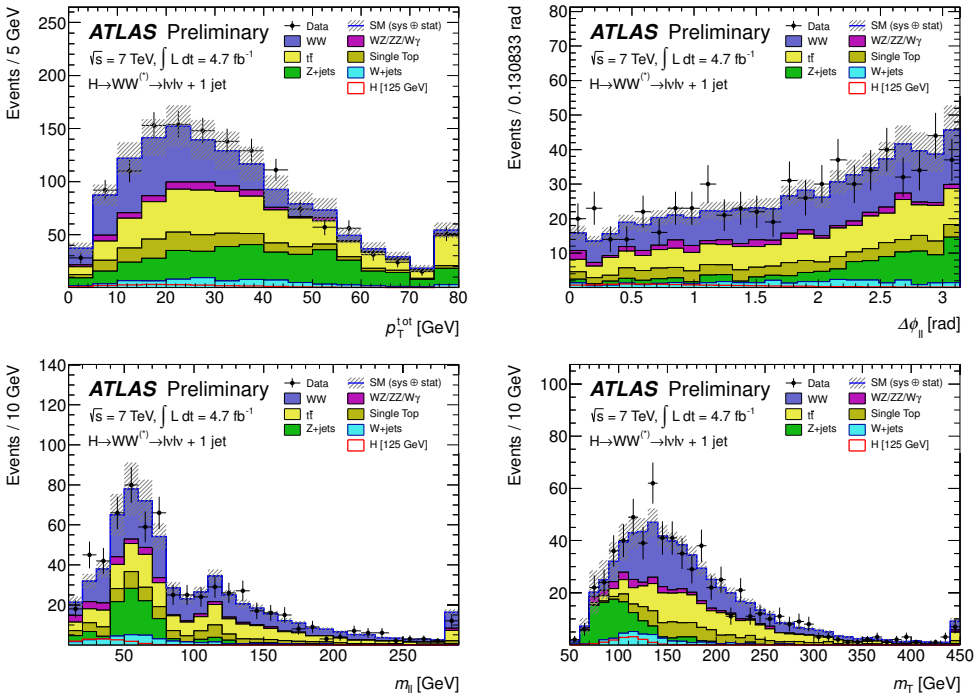

Figure 9: Kinematic distributions in the $H+$ 1-jet channel, after preselection and b-jet veto criteria for $p_{\mathrm{T}}^{\mathrm{tot}}$ (top left), and before the application of the $m_{\ell\ell}$ cut for $\Delta\phi_{\ell\ell}$ (top right), $m_{\ell\ell}$ (bottom left), m_{T} (bottom right). The lepton flavours are combined. The signal shown is for $m_H = 125$ GeV. The hashed area indicates the total uncertainty on the background prediction. The final bin includes the overflow.

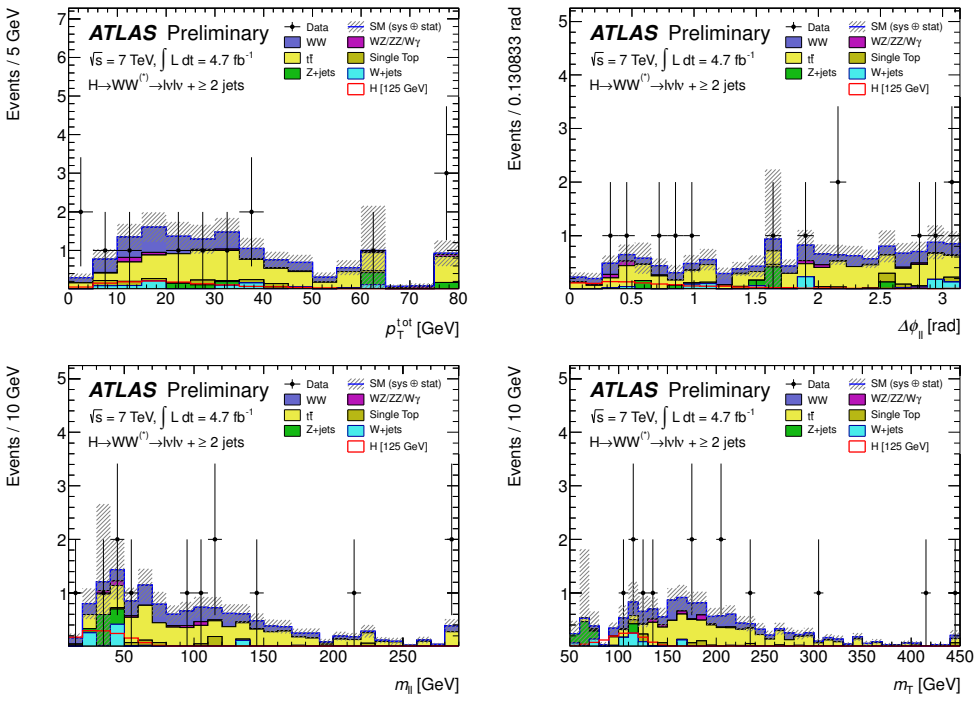

Figure 10: Kinematic distributions in the $H+$ 2-jet channel, before the application of the $m_{\ell\ell}$ cut: $p_{\mathrm{T}}^{\mathrm{tot}}$ (top left), $\Delta\phi_{\ell\ell}$ (top right), $m_{\ell\ell}$ (bottom left), m_{T} (bottom right). The lepton flavours are combined. The signal shown is for $m_H = 125$ GeV. The hashed area indicates the total uncertainty on the background prediction. The final bin includes the overflow.

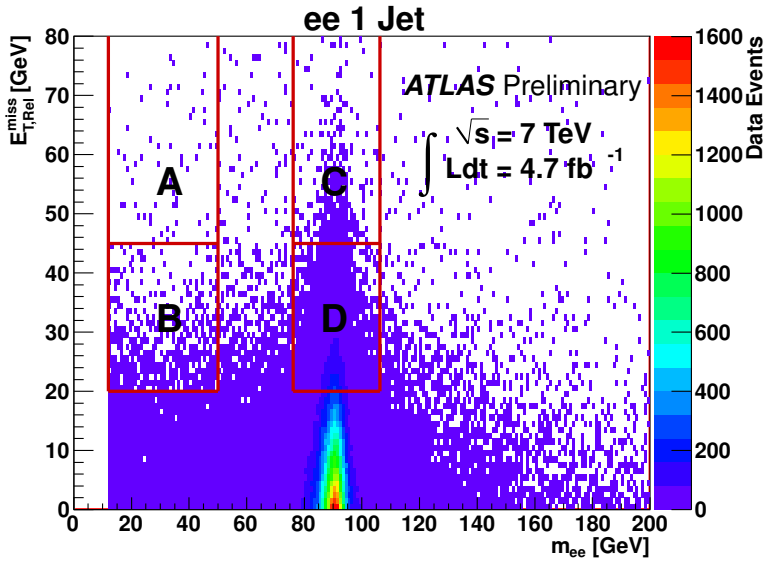

Figure 11: Ranges in the ($m_{\ell\ell}$, $E_{\mathrm{T,rel}}^{\mathrm{miss}}$) plane used to estimate the Z/γ^*+jets background in the ee and $\mu\mu$ channels, as described in Section 5. The distribution shown is that for the ee $H+$ 1-jet channel. The background in the signal region A is obtained by scaling the events in region B (after background subtraction), with the ratio of events in regions C and D.

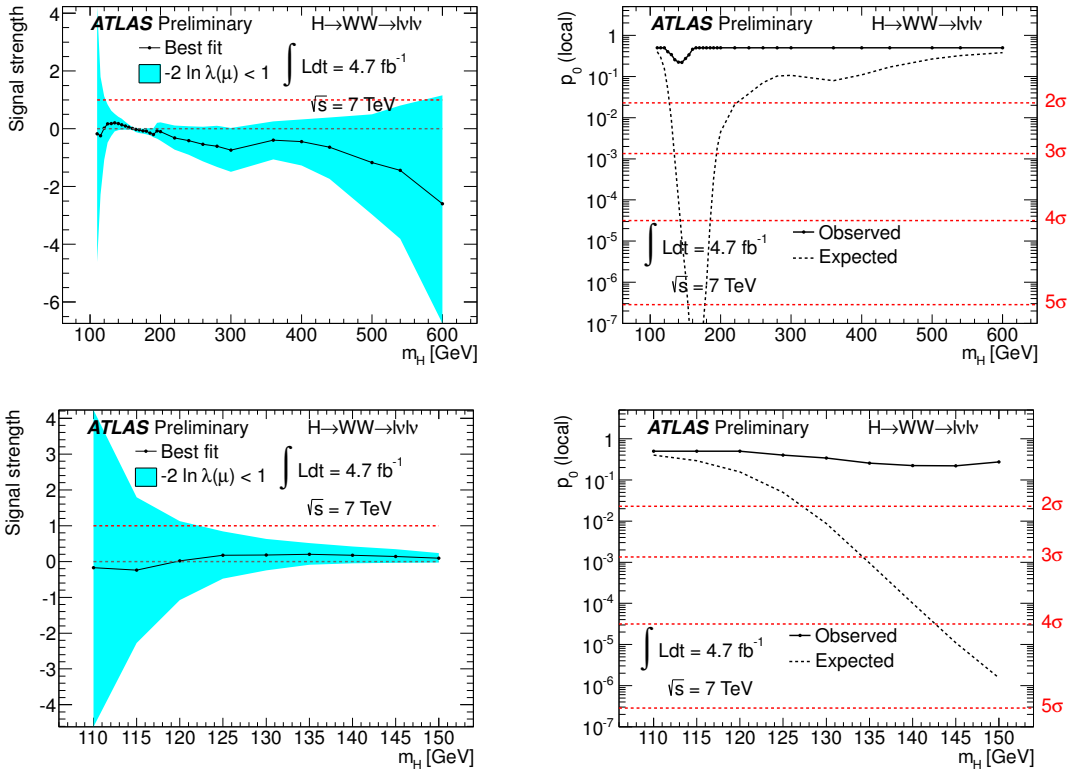

Figure 12: Top left: fitted signal strength parameter (μ) as a function of m_H for the whole mass range. Top right: expected (dashed) and observed (solid) probabilities for the background-only scenario as a function of m_H. The bottom plots show the same information restricted to the region $m_H < 150$ GeV.